The Astrophysical Journal, 577:120–132, 2002 September 20

THE DISTANT TYPE Ia SUPERNOVA RATE

R. Pain,[1] S. Fabbro,[1,2] M. Sullivan,[3] R. S. Ellis,[4,5] G. Aldering,[6] P. Astier,[1] S. E. Deustua,[6] A. S. Fruchter,[7] G. Goldhaber,[6,8] A. Goobar,[9] D. E. Groom,[6] D. Hardin,[1] I. M. Hook,[10] D. A. Howell,[6] M. J. Irwin,[4] A. G. Kim,[6] M. Y. Kim,[6] R. A. Knop,[6] J. C. Lee,[6,11] C. Lidman,[12] R. G. McMahon,[4] P. E. Nugent,[6] N. Panagia,[7] C. R. Pennypacker,[6,13] S. Perlmutter,[6,8] P. Ruiz-Lapuente,[14] K. Schahmaneche,[1] B. Schaefer,[15,16] and N. A. Walton[4]
(The Supernova Cosmology Project)
Received 2001 May 4; accepted 2002 May 22

ABSTRACT

We present a measurement of the rate of distant Type Ia supernovae derived using four large subsets of data from the Supernova Cosmology Project. Within this fiducial sample, which surveyed about 12 deg^2, 38 supernovae were detected at redshifts 0.25–0.85. In a spatially flat cosmological model consistent with the results obtained by the Supernova Cosmology Project, we derive a rest-frame Type Ia supernova rate at a mean redshift $z \simeq 0.55$ of $1.53^{+0.28+0.32}_{-0.25-0.31} \times 10^{-4}\ h^3\ \mathrm{Mpc}^{-3}\ \mathrm{yr}^{-1}$ or $0.58^{+0.10+0.10}_{-0.09-0.09}\ h^2$ SNu (1 SNu = 1 supernova per century per $10^{10}\ L_{B\odot}$), where the first uncertainty is statistical and the second includes systematic effects. The dependence of the rate on the assumed cosmological parameters is studied and the redshift dependence of the rate per unit comoving volume is contrasted with local estimates in the context of possible cosmic star formation histories and progenitor models.

Subject headings: galaxies: evolution — galaxies: high-redshift — supernovae: general

1. INTRODUCTION

Recent observational efforts to detect high-redshift supernovae (SNe) have clearly demonstrated their value as cosmological probes. For the primary purpose of constraining the cosmic expansion history, the Supernova Cosmology Project (SCP) developed a scheduled search–and–follow-up technique that allows the systematic, on-demand discovery and follow-up of "batches" of high-redshift SNe (Perlmutter et al. 1995b). Such batch discoveries of SNe over the following years have led to the construction of two largely independent Hubble diagrams, one by the SCP (Perlmutter et al. 1997a, 1998, 1999) and one by the High-z Supernova Team (Garnavich et al. 1998; Schmidt et al. 1998; Riess et al. 1998), both of which indicate a significant, nonzero cosmological constant.

The batch discovery technique also provides well-controlled search conditions that make it possible to measure the *rate of occurrence* of distant SNe. In Pain et al. (1996, hereafter Paper I), we presented the first such measurement using this technique. The distant SN rate, and its comparison with the nearby SN rate, can provide a diagnostic of the cosmic star formation history (SFH) and metal enrichment at high redshift, as well as a better understanding of possible Type Ia supernova (SN Ia) progenitor models (Madau, Della Valle, & Panagia 1998; Yungelson & Livio 1998). Obtaining a broader understanding of the nature and origin of high-redshift SNe will further improve and refine our use of SNe as cosmological probes.

The local SN Ia rate has recently been reported for two samples, one with $z \simeq 0.01$ (Cappellaro, Evans, & Turatto 1999) based on visual and photographic plates searches, and another at $z \simeq 0.1$ (Hardin et al. 2000) based on CCD searches. In Paper I, we presented the SN Ia rate at intermediate redshift ($z \simeq 0.4$) using three SNe Ia discovered with the 2.5 m Isaac Newton Telescope (INT). In the current paper we report a refined measurement based on an enlarged sample of 38 SNe Ia, spanning the redshift interval 0.25–0.85, discovered over the course of four observing runs at the Cerro Tololo 4 m telescope. The new sample allows us, for the first time, to place constraints on the important question of possible evolution in the rate.

The method we adopt to calculate the SN rate is described in detail in Paper I and contains two components. The first is the estimation of the SN detection efficiency and hence the "control time" (the effective time during which the survey is sensitive to a Type Ia event). We have studied our

[1] Laboratoire de Physique Nucléaire et de Hautes Energies, Universités Paris 6 and 7, Paris, France.
[2] Now at Instituto Superior Técnico, Av. Rovisco Pais, 1049-001 Lisbon, Portugal.
[3] Department of Physics, University of Durham, South Road, Durham DH1 3LE, UK.
[4] Institute of Astronomy, University of Cambridge, Madingley Road, Cambridge CB3 0HA, UK.
[5] California Institute of Technology, Pasadena, CA 91125.
[6] E. O. Lawrence Berkeley National Laboratory, Berkeley, CA 94720.
[7] Space Telescope Science Institute, 3700 San Martin Drive, Baltimore, MD 21218.
[8] Center for Particle Astrophysics, University of California at Berkeley, 301 Le Conte Hall, Berkeley, CA 94720-3411.
[9] Department of Physics, Stockholm University, Sweden.
[10] Department of Physics, Oxford University, Keble Road, Oxford OX1 3RH, UK.
[11] Now at Massachusetts Institute of Technology, Center for Space Research, 70 Vassar Street, Building 37, Cambridge, MA 02139.
[12] European Southern Observatory, La Silla, Chile.
[13] Space Sciences Laboratory, Department of Astronomy, University of California at Berkeley, 601 Campbell Hall 3411, Berkeley, CA 94720-3411.
[14] Department of Astronomy, University of Barcelona, Av. Diagonal 647, Barcelona 8028, Spain.
[15] Department of Astronomy, Yale University, P.O. Box 208101, New Haven, CT 06520-8101.
[16] Current address: University of Texas at Austin, Austin, TX 78712-1083.

detection efficiency as a function of magnitude and SN–to–host galaxy surface brightness ratio using Monte Carlo techniques. The second part estimates the comoving volume and total stellar luminosity to which our SN survey is sensitive. We have computed the total galaxy luminosity from galaxy counts estimated from the Canada-France Redshift Survey (CFRS) and, independently, from recent parameterizations of the type-dependent field galaxy luminosity function (LF) and its redshift evolution. In combination, both aspects then yield an accurate determination of the SN Ia rate at a mean redshift of $z \simeq 0.55$.

A plan of the paper follows. In § 2 we discuss the new SN data set, and in § 3 we introduce our methodologies for estimating the control time and detection efficiencies. We reach significantly fainter detection limits compared to those of Paper I. In § 4 we introduce the formalism for determining the survey comoving volume and in § 5 various ways for estimating the accessible total stellar luminosity. This allows us to estimate the intermediate-redshift SN rate in SNu (1 SNu = 1 supernova per century per 10^{10} $L_{B\odot}$). We discuss the various components of the uncertainties, statistical and systematic, in § 6 and interpret our results in the context of local estimates and cosmic star formation histories in § 7.

2. THE DATA SETS

For this analysis, we have studied four independent data sets of roughly equal size, totaling 219 similar search fields. These fields were observed in 1995 November and December (set A), 1996 February and March (set B), 1997 February and March (set C), and finally 1997 November and December (set D), all using the Cerro Tololo 4 m telescope in Chile. The data sets were obtained as part of the search for high-redshift SNe conducted by the SCP. These images are suitable for a determination of the SN rate since they were obtained under similar conditions at one telescope and therefore form well-defined, homogeneous sets.

Sets A and B were obtained using the 2048^2 pixel prime-focus CCD camera, whereas sets C and D were obtained with the 4×2048^2 pixel Big Throughput Camera (BTC; Wittman et al. 1998). The projected pixel size is $\simeq 0\farcs43$ in both cases, giving an image size of approximately $16' \times 16'$ (or $4 \times 16' \times 16'$ with the BTC). Exposure times were 2×600 s or more in the Kron-Cousins R filter, and the individual images reach a point-source 3 σ magnitude limit ranging from $R = 22.5$ to 24.5 mag. Seeing was typically around $1''$. The fields lie in the range $0^h < \alpha < 15^h$, $\delta > -10°$, avoiding the Galactic plane ($|b| \gtrsim 30°$). A few of the fields were selected as a result of the presence of a high-redshift cluster. The effect of the presence of clusters in the survey fields is taken into account in the calculation of the SN rate (see § 4).

For all fields, a first-look "reference" image was obtained followed by a second look "search" image 2–3 weeks later. The useful solid angle of this data set is defined by the overlap region of the original set of reference images with the search images. The total useful solid angle covered in this study is $\simeq 12$ deg^2. The "reference" images were subtracted from the "search" images after convolution to match the seeing of the worst image and scaling in intensity. The resulting difference image for each field was searched for SN candidates. Table 1 gives the coordinates of the fields together with the SN detection limit and the color excess $E(B-V)$ derived from Schlegel, Finkbeiner, & Davis (1998).

TABLE 1
DATA SETS A THROUGH D

Name (1)	R.A. (2000.0) (2)	Decl. (2000.0) (3)	Detection Limit[a] (4)	$E(B-V)$ (5)
A-1.....	01 04 18.51	07 46 03.9	22.1	0.025
A-2.....	03 07 51.40	10 39 42.9	22.7	0.099
A-3.....	03 36 59.00	00 25 12.7	22.8	0.114
A-4.....	03 15 48.75	−01 34 39.4	23.1	0.031
A-5.....	03 42 32.38	17 30 38.9	22.5	0.128
A-6.....	01 56 55.65	07 42 58.2	23.1	0.040
A-7.....	01 55 00.61	07 53 37.1	23.0	0.046
A-8.....	01 56 28.73	08 07 11.5	23.1	0.043
A-9.....	01 54 47.22	07 55 15.0	23.0	0.041
A-10.....	01 54 38.32	07 59 21.6	23.2	0.044
A-11.....	01 54 28.74	08 17 10.7	23.2	0.044
A-12.....	01 55 45.31	08 15 19.3	23.1	0.038
A-13.....	01 53 21.74	07 33 23.9	23.0	0.033
A-14.....	01 53 32.34	07 57 34.0	22.9	0.038
A-15.....	01 53 34.85	08 18 02.8	23.0	0.052
A-16.....	01 33 57.62	06 20 25.0	23.5	0.044
A-17.....	01 43 10.43	02 32 17.6	23.0	0.023
A-18.....	01 49 38.77	02 04 49.0	22.9	0.048
A-19.....	02 03 05.76	01 55 26.9	23.0	0.029
A-20.....	02 06 59.11	06 52 13.1	22.7	0.035
A-21.....	02 37 45.13	03 43 23.6	22.6	0.035
A-22.....	04 59 02.18	07 57 55.9	23.2	0.235
A-23.....	05 16 46.29	14 48 35.0	23.4	0.688
A-24.....	08 55 10.82	08 01 16.7	23.2	0.018
A-25.....	08 26 59.23	04 35 37.6	23.9	0.027
A-26.....	08 52 05.41	02 15 22.2	21.8	0.034
A-27.....	02 08 11.00	−13 29 16.8	23.2	0.019
A-28.....	01 35 40.23	04 23 32.5	23.0	0.023
A-29.....	01 37 05.37	04 17 45.2	23.2	0.022
A-30.....	01 37 37.86	04 19 14.0	23.1	0.021
A-31.....	01 38 50.55	04 21 07.5	23.2	0.019
A-32.....	01 39 59.01	04 21 19.0	23.1	0.021
A-33.....	01 40 51.70	04 21 45.3	23.2	0.022
A-34.....	01 35 43.81	04 30 38.4	22.9	0.025
A-35.....	01 36 28.77	04 33 17.2	22.9	0.021
A-36.....	01 37 24.50	04 36 01.0	23.1	0.021
A-37.....	01 38 41.33	04 27 02.2	22.4	0.019
A-38.....	01 39 16.44	04 37 20.6	23.2	0.022
A-39.....	01 40 44.93	04 32 54.6	23.2	0.019
A-40.....	03 00 56.51	00 28 36.3	22.9	0.041
A-41.....	03 03 00.71	00 36 25.2	22.7	0.031
A-42.....	03 03 58.40	00 29 33.5	23.1	0.029
A-43.....	03 00 27.57	00 52 40.2	23.1	0.041
A-44.....	03 01 59.24	00 51 06.8	23.0	0.033
A-45.....	03 02 36.56	00 49 50.4	22.8	0.033
A-46.....	03 01 43.69	01 01 21.7	22.9	0.036
A-47.....	03 22 18.03	−04 58 15.8	23.1	0.032
A-48.....	03 23 13.26	−04 58 00.5	23.1	0.034
A-49.....	05 12 33.79	−05 28 24.2	23.5	0.094
A-50.....	05 14 08.04	−05 25 26.9	23.0	0.146
A-51.....	05 15 06.22	−05 22 47.4	23.5	0.142
A-52.....	05 15 42.22	−05 27 40.8	23.3	0.174
A-53.....	05 16 38.77	−05 19 49.7	23.5	0.184
A-54.....	05 17 29.27	−05 23 23.6	23.3	0.191
A-55.....	05 18 32.34	−05 27 45.2	23.1	0.199
A-56.....	05 11 55.21	−05 08 31.1	23.5	0.087
A-57.....	05 13 13.89	−05 15 08.8	23.5	0.125
A-58.....	05 14 28.75	−05 15 52.9	23.4	0.155
A-59.....	05 15 56.36	−05 09 13.4	23.5	0.132
A-60.....	05 16 21.30	−05 07 41.7	23.5	0.120
A-61.....	05 15 19.46	−04 52 38.5	23.4	0.123
A-62.....	05 15 26.23	−04 58 06.4	23.2	0.117
A-63.....	05 16 54.53	−04 55 53.2	23.5	0.091

TABLE 1—*Continued*

Name (1)	R.A. (2000.0) (2)	Decl. (2000.0) (3)	Detection Limit[a] (4)	$E(B-V)$ (5)
A-64.....	08 13 58.35	10 02 08.8	23.2	0.038
A-65.....	08 16 03.00	10 02 51.0	23.3	0.040
A-66.....	08 17 32.60	10 07 47.0	23.0	0.035
A-67.....	08 14 56.29	10 11 05.5	22.7	0.042
A-68.....	08 15 42.78	10 22 30.0	23.2	0.039
A-69.....	08 16 58.45	10 45 50.5	23.2	0.037
B-1.....	12 40 43.23	−07 09 48.5	23.4	0.038
B-2.....	12 34 43.21	−09 24 52.4	23.3	0.036
B-3.....	11 21 33.31	00 07 09.2	23.5	0.043
B-4.....	10 40 17.51	−06 59 30.4	22.8	0.049
B-5.....	08 54 58.96	08 09 17.1	23.0	0.017
B-6.....	10 16 42.40	−01 10 36.9	22.4	0.031
B-7.....	08 51 34.90	02 16 35.6	22.9	0.032
B-8.....	09 00 20.78	03 53 52.6	22.6	0.036
B-9.....	12 26 48.93	11 16 46.7	22.6	0.033
B-10.....	12 57 57.65	−00 38 19.8	23.2	0.029
B-11.....	11 32 24.04	−03 07 30.4	23.3	0.035
B-12.....	13 17 29.17	−04 16 06.3	22.3	0.024
B-13.....	14 18 44.14	02 52 33.1	23.1	0.027
B-14.....	14 19 32.93	02 59 42.6	23.1	0.026
B-15.....	14 21 00.04	02 53 38.3	23.1	0.024
B-16.....	14 21 19.88	02 55 10.4	23.1	0.026
B-17.....	14 22 58.40	02 58 46.6	23.0	0.027
B-18.....	14 23 54.41	02 57 59.6	23.1	0.026
B-19.....	14 24 06.19	02 57 29.6	23.4	0.026
B-20.....	15 04 35.18	02 55 42.4	23.3	0.028
B-21.....	15 05 51.60	02 53 51.3	23.4	0.030
B-22.....	15 06 13.93	02 56 24.9	23.3	0.029
B-23.....	09 56 32.84	03 16 54.2	22.6	0.037
B-24.....	09 57 24.31	03 20 11.9	22.2	0.042
B-25.....	09 58 19.95	03 20 54.6	22.8	0.043
B-26.....	09 56 44.60	03 08 34.8	22.8	0.038
B-27.....	10 31 46.59	00 06 42.0	22.6	0.038
B-28.....	10 30 51.46	−00 06 44.0	22.5	0.041
B-29.....	11 23 37.67	00 47 12.5	23.4	0.041
B-30.....	11 24 39.81	00 43 27.8	23.1	0.040
B-31.....	13 17 50.56	−00 09 31.9	23.0	0.021
B-32.....	13 19 39.82	−00 06 45.5	22.6	0.024
B-33.....	13 19 59.64	−00 07 03.1	23.2	0.025
B-34.....	13 21 22.75	−00 08 11.1	23.4	0.025
B-35.....	13 22 20.39	−00 07 01.9	23.6	0.027
B-36.....	13 23 04.56	−00 07 10.9	23.5	0.033
B-37.....	13 24 26.99	−00 06 39.7	23.6	0.034
B-38.....	16 06 06.38	06 40 14.7	22.9	0.045
B-39.....	16 05 59.89	06 23 30.0	23.3	0.049
B-40.....	16 07 16.97	06 26 15.2	22.9	0.046
B-41.....	16 08 38.64	06 29 30.6	23.0	0.052
B-42.....	16 09 07.04	06 22 04.6	23.2	0.051
B-43.....	16 09 43.78	06 26 41.9	22.9	0.051
B-44.....	16 10 22.41	06 01 20.1	23.0	0.048
B-45.....	16 10 47.22	05 58 39.0	23.4	0.050
B-46.....	16 11 59.78	06 00 36.4	23.1	0.060
C-1[b].....	08 15 49.75	10 00 22.4	23.8	0.040
C-5.....	08 56 15.99	04 41 47.7	23.1	0.021
C-9.....	08 59 04.49	04 39 53.8	23.4	0.027
C-13.....	08 58 34.19	04 00 32.8	22.9	0.029
C-17.....	11 23 28.58	00 56 39.2	24.2	0.043
C-21.....	11 31 30.08	−02 45 35.0	24.0	0.041
C-25.....	11 33 28.88	−02 42 35.2	24.0	0.037
C-29.....	11 31 22.77	−03 17 59.8	24.1	0.034
C-33.....	13 20 22.31	00 01 09.1	24.1	0.025
C-37.....	13 22 37.16	00 03 11.9	24.5	0.026
C-41.....	14 22 02.21	02 51 51.7	24.0	0.026
C-45.....	14 24 46.62	02 55 49.2	23.9	0.024

TABLE 1—*Continued*

Name (1)	R.A. (2000.0) (2)	Decl. (2000.0) (3)	Detection Limit[a] (4)	$E(B-V)$ (5)
C-49.....	08 29 48.58	05 00 52.2	19.6	0.019
C-53.....	10 32 16.36	−00 12 47.3	23.2	0.045
C-57.....	10 35 10.67	00 27 23.7	23.3	0.031
D-1[b].....	08 58 47.18	04 27 12.9	24.3	0.026
D-5	09 01 26.27	04 27 37.9	24.5	0.027
D-9	09 01 41.03	03 49 21.3	24.6	0.048
D-13.....	05 37 35.18	−02 53 03.5	22.7	0.048
D-17.....	05 37 33.80	−03 30 45.1	18.6	0.065
D-21.....	05 35 40.87	−02 26 18.1	24.0	0.058
D-25.....	05 35 37.78	−02 57 02.2	24.1	0.051
D-29.....	05 34 46.79	−03 27 48.5	24.4	0.045
D-33.....	05 33 31.54	−02 14 40.9	24.1	0.056
D-37.....	08 59 20.58	03 55 52.7	24.2	0.031
D-41.....	08 57 00.27	04 01 24.3	23.6	0.026

NOTE.—Units of right ascension are hours, minutes, and seconds, and units of declination are degrees, arcminutes, and arcseconds. Col. (1): Field name. Col. (2): Right ascension (equinox 2000.0). Col. (3): Declination (equinox 2000.0). Col. (4): SN detection limit. Col. (5): Color excess from Schlegel et al. 1998.

[a] Defined as the magnitude above which the SN detection efficiency drops below 50% of the maximum detection efficiency in the field.

[b] For fields C and D observed with the Big Throughput Camera (4 CCDs), we provide information for one of the CCDs.

2.1. *Supernova Detection and Identification*

The original search for SNe was performed with a view to measure the cosmological parameters Ω_M and Ω_Λ (Perlmutter et al. 1999). The detection of SNe was done in three steps:

1. The selection of transient events detected on the subtraction images with a signal-to-noise ratio cut of 3.5 σ and a 15% cut on the ratio of the candidate flux and the host galaxy aperture flux at the candidate position. The latter cut had to be applied to remove systematics from subtraction residuals.
2. The rejection of statistical fluctuations, cosmic rays, and asteroids with coincidences built from the multiple images of the same field taken at both epochs (" reference " and " search ").
3. The rejection of the remaining spurious candidates generated by hot or dead pixels, flat field defects, or bad subtractions with a visual inspection of each subtraction.

Altogether, 58 candidates passed the cuts in the original search, and all but one were observed spectroscopically with the Keck Low Resolution Imaging Spectrometer (LRIS; Oke et al. 1995). The one remaining candidate was not followed up spectroscopically because of a lack of telescope time (and was thus not included in the cosmological parameter study in Perlmutter et al. 1999). Its light curve, however, is consistent with that of an SN Ia at redshift $z \simeq 0.7$.

Of the 57 objects with spectral information, four were classified as " non-SNe " (QSO/AGN) and the 53 remaining retained as possible SNe (Perlmutter et al. 1995a, 1996, 1997b, 1997c).

For the purpose of measuring the rate, a new search was performed on the same subtractions, slightly raising the signal-to-noise ratio cut (typically to 5 σ) in order to ensure good control of the SN detection efficiencies. A total of 46 candidates remained at this stage (including the four " non-

SNe''), of which five were spectroscopically identified as "non-Ia" (II or QSO/AGN or Ib/c) and 37 as "possible SNe Ia." SNe II were identified by the presence of hydrogen or by their very blue featureless spectrum, while SNe Ib/c were identified by the absence of hydrogen and Si II or S II lines and the presence of narrow Ca II H and K features. The following criteria were then used to identify the SN Ia (I. Hook et al. 2002, in preparation): (1) presence of Si II in the spectrum; for redshifts greater than $z \sim 0.5$, Si II λ4130 was used since Si II λ6150 is beyond the spectroscopic range of LRIS; (2) presence of the S II "W" feature at $\sim$5500 Å when detected; (3) the large width of the $\sim$4000 Å Ca II feature, characteristic of SNe Ia.

A total of 28 candidates were identified as SNe Ia using the above criteria, leaving only nine for which the spectra had signal-to-noise ratios too low to distinguish among Type I subtypes. These nine objects were discovered during the first two runs (sets A and B) and observed spectroscopically under nonoptimal weather conditions. On the contrary, all objects discovered during the two other runs (sets C and D) were observed with good signal-to-noise ratios. None of these events were classified as Ib/c. Considering the fact that all four sets have roughly equal sizes and were searched using the same procedures, this implies that the contamination by non–SNe Ia in sets A and B is likely to be comparable, i.e., less than 10%. Two candidates have an E/S0 host type (M. Sullivan et al. 2002, in preparation), which is a strong indicator of the SN being of Type Ia. Adding the facts that the light curves of these partially identified objects resemble a Type Ia light curve at the observed redshift and that their peak magnitude is close to a Type Ia peak magnitude, we classified all nine objects as "probable Ia." These nine events together with the one that was not observed spectroscopically were therefore retained for the rate analysis, but the possibility that one of these objects may not be an SN Ia was used to estimate the effect of possible misidentification of SN type on the systematic uncertainty (§ 6).

Altogether, 38 SNe Ia with redshifts ranging from 0.25 to 0.85 were retained from the 58 discovered. Redshifts were determined from spectra of the host galaxies. The properties of all 38 SNe Ia used in this analysis are summarized in Table 2.

3. DETECTION EFFICIENCIES AND CONTROL TIME

The data presented here were obtained with an observing strategy designed to measure the cosmological parameters Ω_M and Ω_Λ by conducting a search for SNe on the rise using a subtraction technique. We followed the procedure introduced in Paper I to calculate the "control time" and detection efficiencies.

3.1. *Supernova Detection Efficiencies*

Detection efficiencies were determined for every search field using Monte Carlo simulations. A synthetic image was created for every field by adding simulated SNe to the search images. Reference images were subtracted from the synthetic search images using exactly the same software and cuts as used for the actual search, and the number of simulated SNe that satisfied the selection criteria was determined. The efficiency derived in this way then naturally accounts for parts of the image that are unusable for the SN search, for example, regions saturated by bright foreground stars. Over 200 simulated SNe were placed on each search image, with a range of apparent magnitude, host galaxy apparent magnitude, and location with respect to host galaxies. Each simulated SN was generated by scaling down and shifting a bright star, with signal-to-noise ratio greater than 50, from the image being studied (it was not necessary to add additional Poisson noise because the dominant noise source is that of the sky). The position relative to the host galaxy was chosen at random from normal distributions with σ equal to the half-width at half-maximum of the gal-

TABLE 2
38 DISTANT TYPE Ia SUPERNOVAE

IAU Name	Geocentric Redshift of SN or Host Galaxy	Approximate Discovery *R* Magnitude	IAU Name	Geocentric Redshift of SN or Host Galaxy	Approximate Discovery *R* Magnitude
1995aq	0.453	22.4	1997ag	0.592	23.2
1995ar	0.497	23.1	1997ai	0.450	22.3
1995as	0.498	23.3	1997aj	0.581	23.8
1995at	0.655	22.7	1997ak	0.347	24.4
1995aw	0.400	22.5	1997al	0.621	23.8
1995ax	0.615	22.6	1997am	0.416	23.4
1995ay	0.480	22.7	1997ap	0.830	24.2
1995az	0.450	24.0	Unnamed[a]	$\sim$0.7	23.5
1995ba	0.388	22.6	1997el	0.636	23.1
1996cf	0.570	22.7	1997em	0.460	23.6
1996cg	0.460	22.1	1997ep	0.462	22.4
1996ch	0.580	23.7	1997eq	0.538	22.4
1996ci	0.495	22.3	1997er	0.466	22.3
1996ck	0.656	23.5	1997et	0.633	23.4
1996cl	0.828	23.6	1997eu	0.592	22.4
1996cm	0.450	22.7	1997ex	0.361	21.4
1996cn	0.430	22.6	1997ey	0.575	22.9
1997ac	0.320	23.1	1997ez	0.778	23.4
1997af	0.579	23.7	1997fa	0.498	22.5

[a] Not observed spectroscopically (see text).

axy independently on both the x- and y-axes. The shift of the scaled bright star relative to the host galaxy was constrained to be an integral number of pixels in order to maintain the pixelized point-spread function.

We reached significantly fainter detection limits during these observations compared to the data in Paper I. Figure 1 shows the fractional number of simulated SNe recovered, as a function of SN detected magnitude, for 12 representative examples among the 219 fields observed. For a typical field the detection efficiency is over 85% for any stellar object brighter than $R = 23.5$. Note that the loss in efficiency at the brightest magnitudes is due to detector saturation for bright sources. The plateau efficiency seen at intermediate magnitudes simply reflects the areal coverage lost as a result of masking of the region surrounding bright stars.

The efficiency depends primarily on the SN magnitude, but the Monte Carlo simulation also permits us to account for the small dependence of SN visibility on the host galaxy surface brightness underlying each SN. This is shown in Figure 2*a*, where the overall SN detection efficiency for set A is plotted as a function of the magnitude difference between the host galaxy aperture flux at the SN position and the SN flux. Figure 2*b* shows the overall SN detection efficiency as a function of the projected distance to the host galaxy center. The detection efficiency does not depend on the SN position relative to the host, demonstrating the ability of image subtraction techniques to detect SNe on the nuclei of galaxies.

3.2. *Control Time*

We computed a control time as a function of redshift and host galaxy magnitude equal to the weighted sum of the number of days during which the SN could be detected, given the time separation of the search and reference

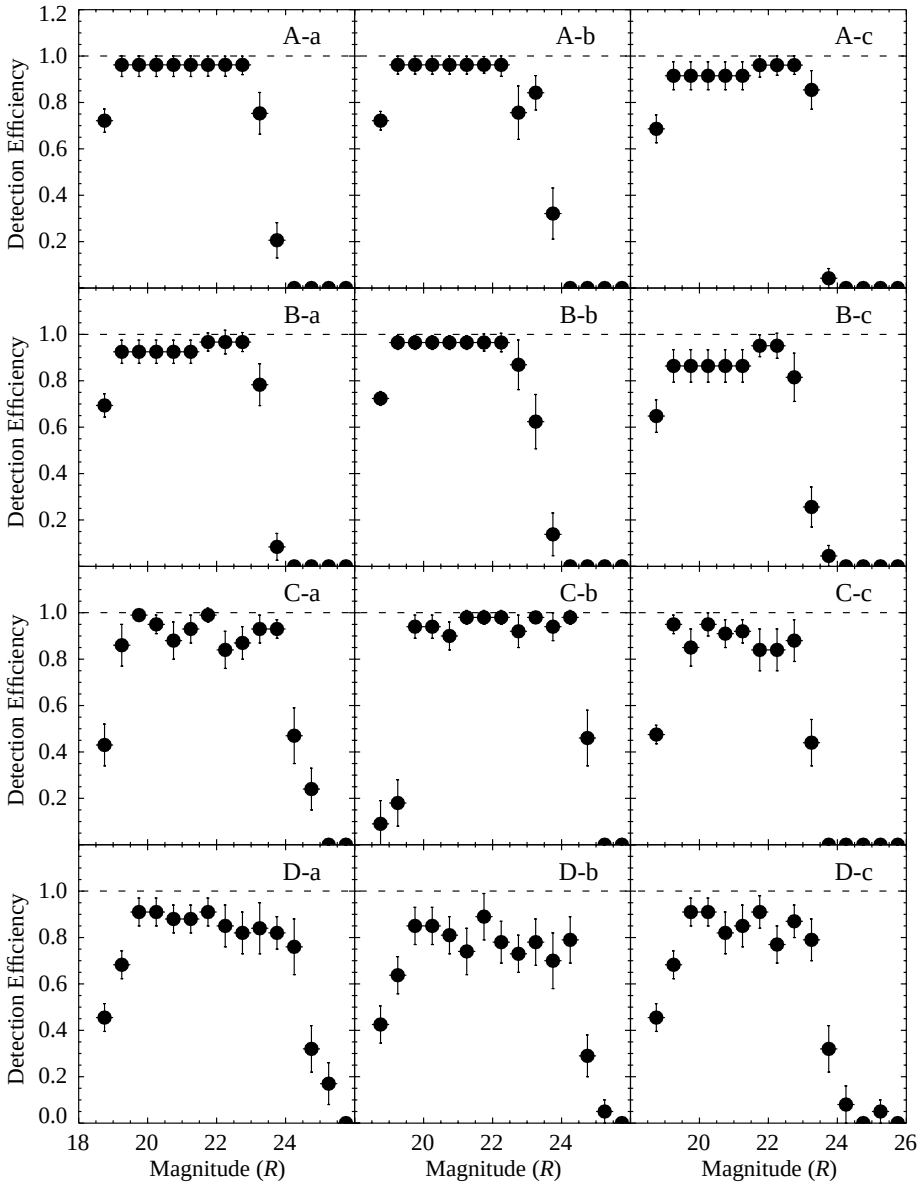

FIG. 1.—Detection efficiency vs. R magnitude of the SN for 12 representative examples among the 219 2k × 2k fields that were searched for SNe. SN 1995as, SN 1996cj, SN 1997ai, and SN 1997ep were discovered on fields A-a, B-a, C-a, and D-a, respectively.

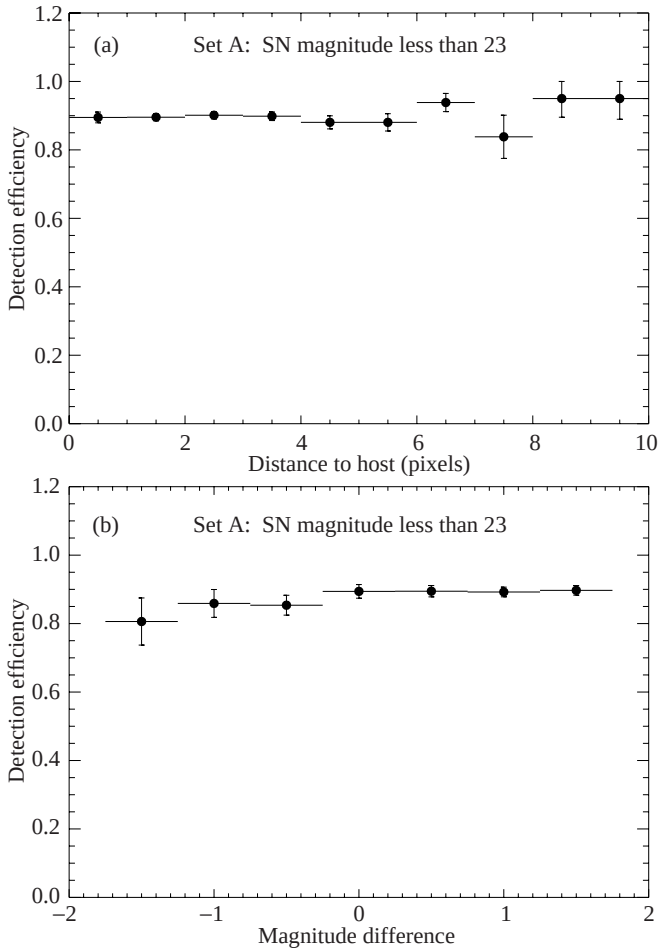

FIG. 2.—(*a*) Detection efficiency vs. projected distance to host galaxy. (*b*) Detection efficiency as a function of magnitude difference between the host galaxy and the SN (host R magnitude − SN R magnitude). In both plots, an overall ∼10% inefficiency is present, as a result of the areal coverage lost by masking the region surrounding bright stars, independently of the distance to the host or the magnitude difference.

images, where the weighting is according to the corresponding detection efficiency.

SN Ia light curves are not unique. The total range for SN Ia B-band peak brightness spans ∼0.5 mag (Saha et al. 1999; Gibson et al. 2000). This has to be taken into account when computing the control time. Furthermore, as first noted by Phillips (1993), brighter SNe also have wider light curves. This correlation between light-curve shape and peak luminosity has the effect of further increasing the "visibility" of brighter objects and therefore the time during which they can be detected. To account for this correlation, the control time was computed, assuming that the SN Ia light curves form a one-parameter family using an approximation for the light-curve shape–luminosity relation following the "stretch factor" method of Perlmutter et al. (1997a). We assumed that the average SN light curve follows the average of the best-fit, time-dilated, and K-corrected Type Ia template (Leibundgut 1988), with the generalized cross-filter K-correction described by Kim, Goobar, & Perlmutter (1996), and that the stretch parameter follows a Gaussian distribution with $\sigma \sim 0.08$ (Perlmutter et al. 1999). The effect of the uncertainties in the light-curve shape–luminosity correction and of the remaining ∼0.15 mag B-band peak luminosity intrinsic scatter on the systematic uncertainty in deriving the SN rates is discussed in § 6.

The SN Ia light curves were calibrated using Landolt standards (Landolt 1992). Since these are observed light curves, in *apparent* magnitudes, no explicit dependence of our rate on H_0, Ω_M, or Ω_Λ is introduced at this stage. Photometric calibration was not available for all the fields. For those fields without calibration (about 25%), zero points were calculated by comparison with E-band (which is close to R band) magnitudes of anonymous stars in the Automated Plate Measuring Facility (APM) POSS I catalog (McMahon & Irwin 1992). A comparison of the APM E magnitudes with CCD R magnitudes was performed using the fields on which SNe had been discovered. The distribution reveals a mean $E-R$ offset of -0.02 mag, with a dispersion of 0.22 mag. Assuming that these fields are representative of the whole data set, we applied a 0.02 mag shift to the APM magnitudes. The uncertainty in the rate introduced by this uncertain calibration is also discussed in § 6.

Galactic extinction was taken into account for each field separately using two different methods. First, we used the Galactic reddening value for each field $E(B-V)$ supplied by D. Burstein (1998, private communication), derived from the analysis of Burstein & Heiles (1982). We applied these to the data assuming $R_V = 3.1$ and $A_R/A_V = 0.751$ (Cardelli, Clayton, & Mathis 1989). For the second method, we computed the extinction using more recent estimations of dust reddening (Schlegel et al. 1998) and $A_R/E(B-V) = 2.63$ (appropriate for the Landolt R filter). Although the individual field reddening values so determined can sometimes differ by a large amount even for our high-latitude survey fields, the net effect on the rate is small as discussed in § 6.

4. SN Ia RATES PER UNIT COMOVING VOLUME

To calculate the observed SN Ia rate per unit comoving volume, we derive the expected redshift distribution of SNe, $N_{\rm exp}(z)$, which is proportional to the observed SN Ia rate, $r_V(1+z)^{-1}$, where r_V is the rest-frame SN rate per unit comoving volume and $(1+z)^{-1}$ accounts for cosmological time dilation. The expected distribution is given by

$$N_{\rm exp}(z) = \frac{r_V}{1+z}\sum_i S_i V(z; H_0, \Omega_M, \Omega_\Lambda)\Delta T_i(z)\ , \qquad (1)$$

where i runs over all the survey fields, S_i is the field solid angle, and $V(z)$ is the comoving volume element at redshift z (formally $d^2V/dz\,dS$), which depends on the cosmological parameters H_0, Ω_M, and Ω_Λ (see, e.g., eq. [26] in Carroll, Press, & Turner 1992). Since the SN detection efficiency depends on the galaxy apparent magnitudes ($R_{\rm gal}$), the control time per field at redshift z [$\Delta T_i(z)$] is computed as $\Delta T_i(z) = \sum_R N_{\rm gal}(z,R)_i \Delta T_i(z, R_{\rm gal})/\sum_R N_{\rm gal}(z,R)_i$, where the sum runs over all possible galaxy apparent magnitudes. Individual control times have been calculated for each field in bins of z and R (the size of the bins used is 0.5 mag in R and 0.1 in z).

A total of 27 of our 219 search fields had been chosen specifically to target high-redshift clusters. Suitable clusters and their redshifts were taken from Gunn, Hoessel, & Oke (1986). Although clusters will be found quite naturally in the SCP wide-field images, it is conceivable that they are overrepresented. For each cluster target field, we therefore

determined the excess number count as a function of R magnitude and clustercentric radius by subtracting the appropriate background field. Assigning the known redshift of the appropriate cluster to the excess populations so determined, the effect on the rate per unit comoving volume was estimated by increasing the comoving volume element at the cluster redshift by the fractional excess of luminosity. The uncertainty in the rate introduced by targeting these high-redshift clusters is estimated in § 6.

4.1. *One-Parameter Fits*

Assuming a constant SN Ia rate as a function of redshift in the region covered by these data, we can perform a maximum likelihood fit of the observed redshift distribution to $N_{\rm exp}$ and hence derive r_V at a mean redshift, $\bar{z} = \int z N_{\rm exp}(z)dz / \int N_{\rm exp}(z)dz$.

The dependence of r_V on the Hubble parameter H_0 is easily factorized (since the comoving volume element scales as H_0^{-3}), but r_V also depends on the cosmological parameters Ω_M and Ω_Λ. At $z = 0.5$, the comoving volume element in a flat universe with $\Omega_\Lambda = 0.7$ is twice that in a flat universe with no cosmological constant. Table 3 gives the results of the fits for different values of Ω_M and Ω_Λ. For a spatially flat cosmological model with $\Omega_M = 0.28$ as measured by the SCP (Perlmutter et al. 1999) and also reported by the High-z Supernova Team from their complete set of spectroscopic SNe Ia (Riess et al. 1998), we obtain

$$r_V = 1.53^{+0.28}_{-0.25}(\text{stat}) \times 10^{-4}\ h^3\ \text{Mpc}^{-3}\ \text{yr}^{-1}\ , \qquad (2)$$

where the error is statistical only at this stage and $h = H_0/100$. Slightly different results for Ω_M have also been reported by both groups depending on the sample retained in the analysis and the method used, and Ω_M has also been measured with different techniques (see, e.g., Peacock et al. 2001). It is therefore interesting to investigate the effect on the rate of changing the values of the cosmological parameters. A closer inspection of the comoving volume element dependence on Ω_M and Ω_Λ shows that, to a good approximation (<5%), this quantity depends only on the difference $\omega = \Omega_M - \Omega_\Lambda$ in our redshift range and for $0.1 < \Omega_M < 1.5$ and $|\omega| < 1.5$. We therefore also provide the result as a function of h and ω and find that the following is a good approximation to our results:

$$r_V(\bar{z} = 0.55) = \left[\left(2.06^{+0.37}_{-0.33}\right)(1 + 0.58\omega)\right] \times 10^{-4}\ h^3\ \text{Mpc}^{-3}\ \text{yr}^{-1}\ , \qquad (3)$$

where the error is again only statistical at this stage.

TABLE 3
SN Ia Rate per Unit Comoving Volume for Different Cosmological Models

Model	Ω_M	Ω_Λ	$\bar{z}_{\rm exp}$[a]	$\bar{z}_{\rm obs}$[b]	r_V[c]	α[d]
One-Parameter Fits						
Λ.....	0.28	0.72	0.53	0.54	$1.53^{+0.28}_{-0.25}$	...
O.....	0.3	0.0	0.52	0.54	$2.42^{+0.44}_{-0.40}$	...
E.....	1.0	0.0	0.52	0.54	$3.25^{+0.58}_{-0.53}$	...
Two-Parameters Fits						
Λ.....	0.28	0.72	0.54	0.54	$1.55^{+0.29}_{-0.30}$	$0.8^{+1.6}_{-1.6}$
O.....	0.3	0.0	0.54	0.54	$2.48^{+0.48}_{-0.48}$	$1.3^{+1.6}_{-1.6}$
E.....	1.0	0.0	0.54	0.54	$3.36^{+0.64}_{-0.64}$	$1.7^{+1.5}_{-1.6}$

Note.—Model Λ: a flat Λ-dominated model consistent with the latest SCP results; model O: a $\Lambda = 0$ universe with $\Omega_M = 0.3$; model E: an Einstein–de Sitter universe.

[a] Expected mean redshift; computed from the expected number of SNe $N_{\rm exp}(z)$ (see text).

[b] Observed mean redshift.

[c] Rate per unit volume ($10^{-4}\ h^3\ \text{Mpc}^{-3}\ \text{yr}^{-1}$) at mean redshift $z = \bar{z}_{\rm exp}$; statistical uncertainty only.

[d] Evolution index (see text and Fig. 4).

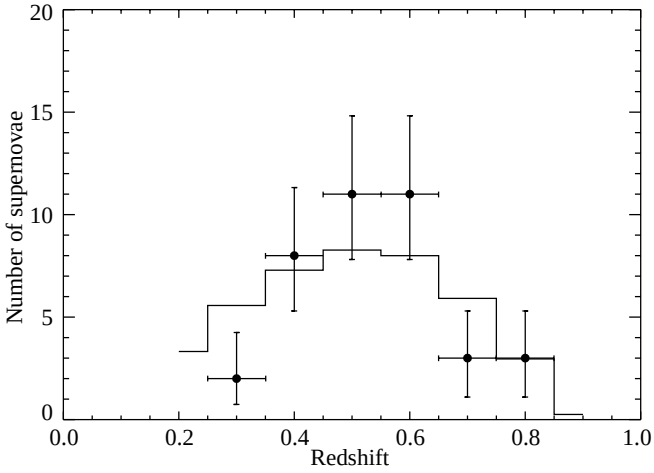

Fig. 3.—SN Ia rate per unit comoving volume: comparison of Monte Carlo calculation (*histogram*) and data (*filled circles*) for the number of observed SNe as a function of redshift. A value of $1.53 \times 10^{-4}\ h^3\ \text{Mpc}^{-3}\ \text{yr}^{-1}$ is assumed for the rate. The prediction assumes no evolution for the rate per unit comoving volume computed with $\Omega_M = 0.28$ and $\Omega_\Lambda = 0.72$.

A comparison of the expected number of SNe and the observed number is shown in Figure 3, where the expected number has been computed assuming no evolution for the rate per unit comoving volume and a flat universe with $\Omega_M = 0.3$. The agreement is quite good, although the expected distribution is slightly flatter.

Using the above determination of r_V, one can compute the theoretical number of SNe that are produced as a function of redshift. This is shown in Figure 4, where the number

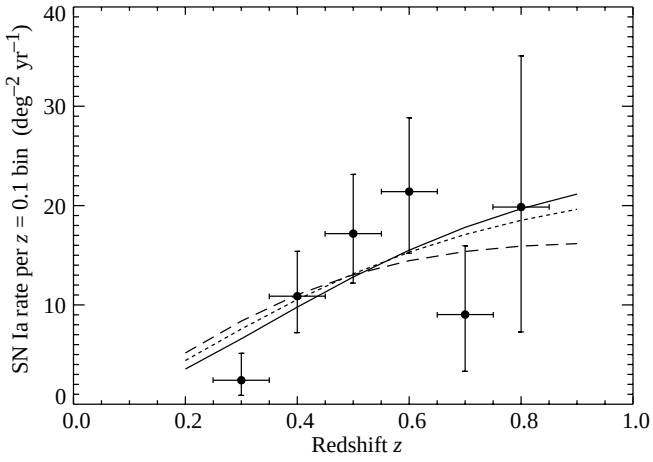

Fig. 4.—Number of SNe Ia per $z = 0.1$ redshift bin per square degree per year as a function of redshift. Overplotted lines are the predictions assuming that the number of SNe is proportional to the comoving volume and adjusted to best fit the observed number of SNe between $z = 0.25$ and 0.85. The solid line is for a comoving volume given by a cosmological model with $\Omega_M = 0.28$ and $\Omega_\Lambda = 0.72$, the dotted line is for $\Omega_M = 0.3$ and $\Omega_\Lambda = 0.0$, and the dashed line is for $\Omega_M = 1.0$ and $\Omega_\Lambda = 0.0$.

of SNe per square degree per year is plotted as well as predictions for different cosmological models adjusted to best fit the observations (assuming that the number scales with comoving volume).

4.2. *Two-Parameter Fits*

In the previous paragraph, the rest-frame SN rate r_V is assumed constant over the redshift range of interest. Several studies have addressed the expected variation of the Ia rate with redshift (see, e.g., Madau et al. 1998; Ruiz-Lapuente & Canal 1998; Sadat et al. 1998). With our enlarged sample spanning the redshift range 0.25–0.85, it is possible to consider an observational constraint on possible rate evolution. We choose to approximate any potential evolution with a power law of the form $r_V(z) = r_{\bar{z}}[(1+z)/(1+\bar{z})]^{\alpha}$, where $r_{\bar{z}}$ is the $z = \bar{z}$ Type Ia rate per unit comoving volume and α is an index of evolution ($\alpha = 0$ indicates no evolution). Equation (1) then becomes

$$N_{\rm exp}(z) = \frac{r_{\bar{z}}(1+z)^{\alpha-1}}{(1+\bar{z})^{\alpha}} \sum_i S_i V(z; H_0, \Omega_M, \Omega_\Lambda) \Delta T_i(z) \ , \quad (4)$$

and we perform a two-parameter fit of $r_{\bar{z}}$ and α.

As before, we perform maximum likelihood fits for a choice of cosmological models. The results are reported in Table 3. As expected, the evolution parameter α depends strongly on the assumed cosmology. A spatially flat Λ-dominated universe (model Λ) favors a solution with little evolution in the SN Ia rate per unit comoving volume, whereas in an Einstein–de Sitter universe (model E) more evolution is permitted.

For the spatially flat case (model Λ) with $\Omega_M = 0.28$, we obtain (Fig. 5)

$$r_{\bar{z}=0.54} = 1.55^{+0.29}_{-0.30} \times 10^{-4} \ h^3 \ {\rm Mpc}^{-3} \ {\rm yr}^{-1}, \quad \alpha = 0.8^{+1.6}_{-1.6} \ , \quad (5)$$

where the error is statistical only.

Although the current data set does not yet allow a stringent constraint to be placed on evolution in the SN Ia rate, with the ever increasing number of SNe found in controlled experiments both at low and intermediate redshifts, the situation will improve quite rapidly. The SN Ia rate will therefore soon become a key ingredient in constraining the astrophysical evolution of host galaxies and in limiting possible progenitor models for SNe Ia.

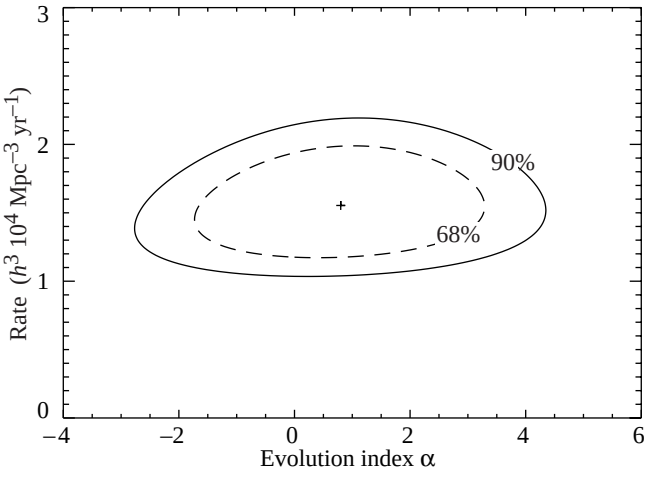

FIG. 5.—Two-parameter maximum likelihood fit of the distant SN Ia rate: 68.3% and 90% confidence regions for the rate per unit comoving volume vs. the evolution index for a comoving volume corresponding to a flat universe with $\Omega_M = 0.28$.

5. SN Ia RATES PER UNIT GALAXY LUMINOSITY

Local estimates of the SN Ia rate are often expressed in the "supernova unit" (SNu), the number of SNe per century per 10^{10} solar luminosities in the rest-frame B band. To compare our distant SN Ia rate with any local determinations, one must either convert the higher redshift rates into SNu or convert the local rates into "events Mpc^{-3} yr^{-1}." In this section we explore the former option.

To estimate our rate in SNu, we proceed as described in Paper I and calculate the expected redshift distribution of SNe Ia given by

$$N_{\rm exp}(z) = \frac{r_L}{1+z} \sum_i \sum_R N_{\rm gal}(z,R)_i \times L_B(z,R; H_0, \Omega_M, \Omega_\Lambda) \Delta T_i(z,R) \ , \quad (6)$$

where i runs over all fields, R is the galaxy apparent R-band magnitude, and L_B is the galaxy rest-frame B-band luminosity in units of $10^{10} \ L_{B\odot}$, which depends on the cosmological parameters H_0, Ω_M, and Ω_Λ.

Since thousands of anonymous high-redshift galaxies are observed in every survey image, it is more difficult than in local SN searches to estimate the number, morphological type, and luminosity distributions of galaxies searched within a given redshift range. To utilize a determination of the total B-band galaxy luminosity, as a function of z and apparent magnitude R, it will also be necessary to have the relevant galaxy K-corrections needed to convert observed R magnitudes into rest-frame B magnitudes.

We approach this determination of $L_B(z,R)$ in two ways. First, as in Paper I, we use observed R-band galaxy counts as a function of redshift and compute from these the rest-frame B-band galaxy luminosity. As a second estimate, we compute $L_B(z,R)$ by integrating recently determined LFs parameterized via the Schechter function. We adopt $M_{B\odot} = 5.48$.

5.1. *Utilizing CFRS Galaxy Counts*

R-band counts as a function of redshift were kindly calculated by S. Lilly (1995, private communication) and are based on the analysis of I-band magnitude–redshift data obtained in the CFRS (Lilly et al. 1995 and references therein). Since the I band is fairly close to the R band, and the magnitude range of the CFRS sample is comparable to that of our data, the extrapolation is small and therefore the dependence of R-band counts on the cosmological parameters is negligible. To compute the rest-frame B-band galaxy luminosities from apparent R magnitudes, we used $B-R$ colors and B-band K-corrections provided by C. Gronwall (1995, private communication; see also Gronwall & Koo 1995).

The SN Ia rate per unit luminosity was then derived using this estimate of $L_B(z,R)$ assuming that the rate per unit luminosity is constant as a function of redshift (an assumption we investigate in § 6). The result is reported in Table 4.

TABLE 4
SN Ia Rate per Unit Luminosity for Different Cosmological Models

Model	Ω_M	Ω_Λ	$\bar{z}_{\rm exp}$[a]	$\bar{z}_{\rm obs}$[b]	r_L[c]
From CFRS Galaxy Counts					
Λ	0.28	0.72	0.56	0.54	$0.63^{+0.11}_{-0.10}$
From Luminosity Functions					
Λ	0.28	0.72	0.58	0.54	$0.58^{+0.10}_{-0.09}$
O	0.3	0.0	0.57	0.54	$0.78^{+0.14}_{-0.13}$
E	1.0	0.0	0.57	0.54	$0.91^{+0.16}_{-0.14}$

Note.—Model Λ: a flat Λ-dominated model consistent with the latest SCP Results; model O: a $\Lambda = 0$ universe with $\Omega_M = 0.3$; model E: an Einstein–de Sitter universe.

[a] Expected mean redshift; computed from the expected number of SNe $N_{\rm exp}(z)$ (see text).

[b] Observed mean redshift.

[c] Rate per unit luminosity (h^2 SNu) at mean redshift $z = z_{\rm exp}$; statistical uncertainty only.

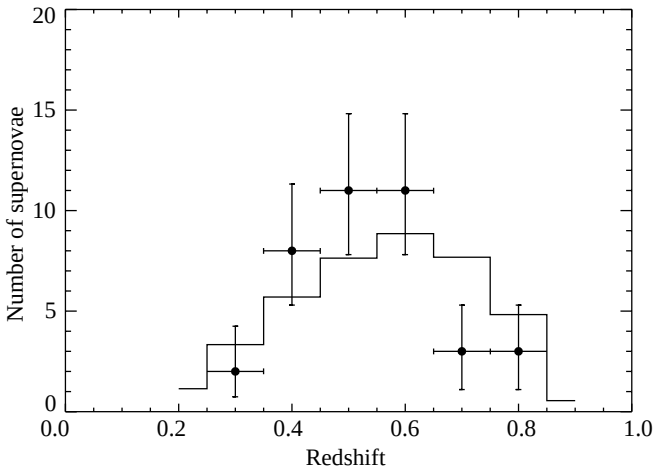

Fig. 6.—SN Ia rate per unit luminosity: comparison of Monte Carlo calculation (*histogram*) and data (*filled circles*) for the observed number of SNe as a function of redshift. The prediction assumes that the rate follows the galaxy luminosity evolution as a function of redshift. A value of 0.58 h^2 SNu is assumed for the rate, and $\Omega_M = 0.28$ and $\Omega_\Lambda = 0.72$ are used.

5.2. *Utilizing Observed Luminosity Functions*

We also estimated $L_B(z, R)$ by integrating recently derived Schechter parameterizations of local field galaxy LFs. We adopted a set of type-dependent LFs covering three broad galaxy classes: E/S0, spiral, and irregular systems. Many type-dependent LFs can be found in the literature (Loveday et al. 1992; Marzke et al. 1998; Folkes et al. 1999), based on many different surveys and classification techniques. The agreement is not particularly good, which renders our calculation somewhat uncertain (see, e.g., Brinchmann 1999). Bearing this in mind, we adopted the LFs of Marzke et al. (1998) as a reasonable "average." Type-dependent *K*-corrections and luminosity evolutionary corrections were adopted from the synthesis models of Poggianti (1997). Finally, to apply these local LFs to higher redshift samples, we also need to account for possible evolution in the LFs themselves. The primary signal is a marked increase with redshift in the abundance of galaxies with irregular morphology, which we account for by introducing an evolution in the space density of irregular systems, adjusted to match the evolution seen by Brinchmann et al. (1998).

Figure 6 shows the expected redshift distribution of SNe Ia, $N_{\rm exp}(z)$, as calculated above for a spatially flat Λ-dominated cosmology (model Λ) assuming that the SN Ia rate per unit luminosity does not evolve. Similar distributions were computed for different cosmological models, and the rest-frame SN rate r_L was derived by fitting the redshift distribution of observed SNe to the expected distribution, $N_{\rm exp}(z)$. Results of these fits are given in Table 4. For a flat universe with $\Omega_M = 0.28$, we find

$$r_L(\bar{z} = 0.55) = 0.58^{+0.10}_{-0.09}({\rm stat})\ h^2\ {\rm SNu}\ . \qquad (7)$$

The value obtained for model Λ is in reasonable agreement (better than 10%) with the value obtained from the CFRS galaxy counts. This is because both estimates of the galaxy luminosity agree very well in the region $z = 0.4$–0.6, where most of the SNe were found. Nevertheless, sizable differences exist in the high-redshift region, where the luminosity derived from the CFRS counts lies significantly below that derived from the direct LF approach, probably as a result of the evolving population of (blue) irregular systems. Since a simple extrapolation was used to estimate the counts at high redshifts from the CFRS data, whereas the luminosity estimated from the parameterization of LFs used more recent high-redshift survey data, the latter should be more realistic.

6. SYSTEMATIC UNCERTAINTIES

With a total of almost 40 SNe Ia, the statistical uncertainty is sufficiently small to demand a careful analysis of possible systematic uncertainties. We estimate these below and summarize their contribution in Table 5.

6.1. *Cosmological Parameters*

With the methods used in this paper to calculate the SN rates, the dependence on the cosmological parameters

TABLE 5
Summary of Uncertainties

Source	δr_V[a]	δr_L[b]
Cosmological parameters.....	$^{+0.25}_{-0.23}$	$^{+0.04}_{-0.03}$
Detection efficiencies.....	±0.12	±0.04
Range of Ia light curves.....	±0.14	±0.05
Field calibration.....	±0.06	±0.02
Cluster contribution.....	±0.05	±0.02
Galaxy extinction.....	±0.02	±0.01
Luminosity estimate.....	...	±0.05
Total systematic uncertainty	$^{+0.32}_{-0.31}$	$^{+0.10}_{-0.09}$
Statistical uncertainty	$^{+0.28}_{-0.25}$	$^{+0.10}_{-0.09}$

Note.—These uncertainties have been computed in a flat Λ-dominated universe using $\Omega_M = 0.28^{+0.10}_{-0.09}$ (see text). No estimate was made of possible systematic uncertainties from host galaxy inclination or extinction.

[a] Uncertainty in the rate per unit volume ($10^{-4}\ h^3\ {\rm Mpc}^{-3}\ {\rm yr}^{-1}$).

[b] Uncertainty in the rate per unit luminosity (h^2 SNu).

appears only in the calculation of the comoving volume element or in estimating the absolute galaxy luminosity. In both cases, the H_0 dependence can be simply factorized. The dependence on Ω_M and Ω_Λ is more difficult to derive, although to a very good approximation ($\simeq$5%) the comoving volume element depends only on the combination $\Omega_M - \Omega_\Lambda$ in our particular redshift range (assuming $0.1 < \Omega_M < 1.5$ and $|\Omega_M - \Omega_\Lambda| < 1.5$; see § 4). In the specific case of a spatially flat cosmology, using the SCP value of $\Omega_M = 0.28^{+0.10}_{-0.09}$, where statistical and systematic uncertainties have been combined, the uncertainty in the event rate becomes $^{+0.25}_{-0.23} \times 10^{-4}$ h^3 Mpc^{-3} yr^{-1}. For the rate per unit luminosity (i.e., in SNu), a simple parameterization on $\Omega_M - \Omega_\Lambda$ is not possible, and for a flat universe with $\Omega_M = 0.28^{+0.10}_{-0.09}$ we find a contribution of $^{+0.04}_{-0.03}$ h^2 SNu.

6.2. *Detection and Identification Efficiencies*

The study of detection efficiencies as a function of SN magnitude is an essential element of this analysis. The detection efficiencies depend on many parameters and vary widely from field to field. Uncertainties were determined using a statistically limited Monte Carlo simulation where 250 fake SNe were added to each image incorporating distribution functions for the galactocentric distance of each SN and the host galaxy magnitude distribution (assumed to be representative of the total galaxy population). The systematic uncertainties were estimated by varying the parameters of the simulation around their nominal values and provide a fractional error on the efficiency of less than 5% or $\pm 0.08 \times 10^{-4}$ h^3 Mpc^{-3} yr^{-1} (± 0.03 h^2 SNu) for each contribution.

During the SCP SN search, differenced images of candidates satisfying loose cuts were scanned by eye and candidates kept or rejected following some quality criteria. This could give some systematic effects that are a priori difficult to estimate precisely. However, for the rate analysis, an automatic procedure was used to retrieve the few hundred fake SNe that were added to each field in order to compute the detection efficiency. This makes it possible to estimate the SCP "scanning" efficiency. Interestingly, we found it to be better than 98% inside the nominal cuts that were set higher than during the actual search.

On the other hand, as discussed in § 3, one SN candidate was not confirmed spectroscopically (see Table 2), and nine others were only spectroscopically identified as Type I and retained as "probable Ia" based on a combination of factors: two have E/S0 hosts and they all have light-curve shape and magnitude at peak compatible with that of an SN Ia. Furthermore, since no Ib/c was identified in sets C and D from the 20 candidates that had spectra, the probability of having an SN Ib/c in sets A and B, where the unidentified candidates have been found, is less than 10% with 90% confidence level. We therefore conclude that at most one of these 10 candidates that could not be positively identified as Ia could be a contaminant.

Altogether, we estimate the systematic uncertainty of both "scanning" efficiency and misclassification effects in the current data set to be $\pm 0.03 \times 10^{-4}$ h^3 Mpc^{-3} yr^{-1} or ± 0.01 h^2 SNu. In combination, uncertainties in the detection efficiencies (detection, scanning, misclassification) translate into an overall systematic uncertainty in the rates of $\pm 0.12 \times 10^{-4}$ h^3 Mpc^{-3} yr^{-1} (± 0.04 h^2 SNu).

6.3. *Range of SN Ia Light Curves*

Control times were calculated following the procedure described in § 3. Noticing that the different implementation of the light-curve shape–luminosity correlation (Hamuy et al. 1996; Phillips et al. 1999; Riess, Press, & Kirshner 1996; Riess et al. 1998; Perlmutter et al. 1997a) can give somewhat different corrections (Leibundgut 2001), we conservatively estimated the systematic uncertainty coming from the light-curve shape–luminosity correlation by varying the "stretch" parameter by 1 σ around its nominal value. The effect on the rate was found to be 0.13×10^{-4} h^3 Mpc^{-3} yr^{-1} (0.04 h^2 SNu). The "intrinsic" scatter of 0.15 mag translates into a change in the rate of 0.03×10^{-4} h^3 Mpc^{-3} yr^{-1} (0.02 h^2 SNu). The overall uncertainty due to the dispersion of SN Ia light curves therefore amounts to $\pm 0.14 \times 10^{-4}$ h^3 Mpc^{-3} yr^{-1} (± 0.05 h^2 SNu) in the rate.

6.4. *Field Calibration*

Measured SN light curves, calibrated with Landolt standards, were used to compute the control time. Efficiency-magnitude curves, also needed to compute the control time, were obtained for all fields calibrated with Landolt standards when available (for 75% of the fields) or with the APM catalog for the others. Errors in the APM calibration of the fields thus alter the determination of the efficiency as a function of magnitude and therefore the control time. This has a sizable effect on the derived SN Ia rate since, at the magnitude of most of our SNe, the detection efficiency varies rapidly with magnitude. We estimated the size of the effect by comparing the discovery magnitudes of our SNe calibrated using Landolt stars and calibrated with the APM, assuming that this was representative of our set of fields. Since only 25% of our fields lack Landolt calibration, the overall effect is reduced. It contributes $\pm 0.06 \times 10^{-4}$ h^3 Mpc^{-3} yr^{-1} (± 0.02 h^2 SNu) to the uncertainty in the rate.

6.5. *Galaxy Luminosity*

The CFRS galaxy counts are based on data that are well matched to our survey in magnitude and redshift range, and only minimal extrapolation was required to convert from the I to R band. The associated uncertainty should be small, and this is supported by the calculation based on using the observed LFs as discussed in § 5 (Table 4). The difference in the two calculations serves as our estimate of the systematic uncertainty here, and this amounts to ± 0.05 h^2 SNu.

6.6. *Contribution from Clusters*

A total of 27 of our 219 search fields had been chosen specifically to target high-redshift clusters. We followed the procedure described in § 4 to account for the excess number counts that could arise from selecting these fields. Although the procedure may suffer large statistical and systematic uncertainties, it only affects a small fraction of the overall search area. We estimated a 50% overall uncertainty in estimating the excess number counts. This translates into less than a 10% uncertainty in calculating the overall contribution to the galaxy counts from clusters, giving a contribution of ± 0.02 h^2 SNu ($\pm 0.05 \times 10^{-4}$ h^3 Mpc^{-3} yr^{-1}) to the uncertainty in the rate. It is likely that this is an overestimate of the uncertainty given that we expect clusters to occur within typical survey fields.

6.7. *Galactic Extinction*

Galactic extinction was computed using two different methods, one taken from Burstein & Heiles (1982), based on emission from atomic neutral hydrogen, and the other from Schlegel et al. (1998), based on dust emission in the far-infrared (FIR). Both groups quote 10% uncertainty in their estimate of the reddening, but differences as big as a factor of 2 in $E(B-V)$ were found. However, the FIR emission maps have much better resolution, which can be important in our case where the reddening has to be known for specific lines of sight. We therefore used Schlegel et al. (1998) as our baseline. The effect on the rate is nevertheless very small since most of our fields were selected to have little or no reddening. Overall the $\pm 10\%$ uncertainty in the reddening translates into an uncertainty in the rate of $\pm 0.02 \times 10^{-4}\ h^3\ \mathrm{Mpc}^{-3}\ \mathrm{yr}^{-1}$ ($\pm 0.01\ h^2$ SNu).

6.8. *Host Galaxy Inclination and Extinction*

The effect of host galaxy inclination on our detection efficiency and galaxy luminosity estimates should be taken into account when calculating SN rates. Cappellaro et al. (1999) recently reestimated the inclination correction factors for relevant nearby searches. In this analysis, both the search technique (in our case subtraction of CCD images) and calculation of the galaxies' luminosities were performed in a different manner than in most local searches, so the inclination effects may not be the same. Inclination and extinction would reduce both the number of SNe detected *and* the galaxy visible luminosity whose effects may partially cancel in estimating the rate. A complete analysis of this effect would require careful modeling of galaxy opacities, which is beyond the scope of this paper. Our result should therefore be directly compared with uncorrected values derived in nearby searches, with particular attention to CCD searches.

6.9. *Brightness Evolution and Intergalactic Dust*

The effect of possible SN Ia brightness evolution or the presence of intergalactic dust was not explicitly taken into account in our derivation of the rates. However, since the SN Ia light curves used to compute the detection efficiencies were calibrated using the observed light curves, a possible difference in the brightness of distant SNe Ia compared to local ones is taken into account whether it is due to evolution or cosmology. On the contrary, the possible presence of intergalactic dust would have the effect of lowering the number of observed SNe. In that case our results would have to be interpreted as a lower limit of the true distant rate.

7. DISCUSSION

We have derived a rest-frame SN Ia rate per unit comoving volume at redshift range 0.25–0.85 ($\bar{z} \simeq 0.55$) of

$$r_V(\bar{z}=0.55) = \left\{\left[2.06^{+0.37}_{-0.33}(\mathrm{stat}) \pm 0.20(\mathrm{syst})\right](1+0.58\omega)\right\} \times 10^{-4}\ h^3\ \mathrm{Mpc}^{-3}\ \mathrm{yr}^{-1}\ , \quad (8)$$

with $\omega = \Omega_M - \Omega_\Lambda$, where the first uncertainty is statistical and the second includes systematic effects that are independent of the systematics arising from the uncertainty on the cosmological parameters.

For a spatially flat universe consistent with the SCP results (i.e., with $\Omega_M = 0.28^{+0.10}_{-0.09}$ [statistical and systematic uncertainty combined quadratically]), we measure

$$r_V^{\mathrm{flat}}(\bar{z}=0.55) = 1.53^{+0.28}_{-0.25}(\mathrm{stat})^{+0.32}_{-0.31}(\mathrm{syst}) \times 10^{-4}\ h^3\ \mathrm{Mpc}^{-3}\ \mathrm{yr}^{-1}\ , \quad (9)$$

where the systematic uncertainty includes the uncertainty on the cosmological parameters.

As most low-redshift determinations of the SN Ia rate are reported in SNu, we also estimate our SN rate in these units. For the rate per unit luminosity, we obtain the following result:

$$r_L(\bar{z}=0.55) = 0.58^{+0.10}_{-0.09}(\mathrm{stat})^{+0.10}_{-0.09}(\mathrm{syst})\ h^2\ \mathrm{SNu} \quad (10)$$

for a flat universe with $\Omega_M = 0.28^{+0.10}_{-0.09}$, and for an Einstein–de Sitter universe, we measure $r_L(\bar{z}=0.55) = 0.94^{+0.16}_{-0.14}(\mathrm{stat}) \pm 0.14(\mathrm{syst})\ h^2$ SNu, in good agreement with our first measurement reported in Paper I, based on the discovery of three SNe Ia at $z \simeq 0.4$, of $r_L(\bar{z}=0.4) = 0.82^{+0.54}_{-0.37}(\mathrm{stat})^{+0.37}_{-0.25}(\mathrm{syst})\ h^2$ SNu.

We have studied the redshift dependence of the rate per unit comoving volume and put constraints on the rate of evolution of the SN Ia rate.

7.1. *Comparison with Other Estimates*

In a recent work to be submitted for publication (Reiss 2002), D. J. Reiss reports values for the SN Ia rate per unit luminosity and per unit volume in excellent agreement with our values ($<1\ \sigma$). His values are based on a sample of 20 SNe at a mean redshift $z \sim 0.49$. Local $z \simeq 0.01$ SN Ia rates have been recently reanalyzed, combining data from five SN searches (see Cappellaro et al. 1999 and references therein). They find $r_L(z=0.01) = 0.36 \pm 0.11\ h^2$ SNu, averaged over all galaxy types. The quoted uncertainties include an estimate of systematic effects. The SN Ia rate at $z \simeq 0.1$ has also been measured by Hardin et al. (2000), who find $r_L(z=0.1) = 0.44^{+0.35+0.13}_{-0.21-0.07}\ h^2$ SNu (here systematic and statistical errors are quoted).

In comparing these rates with our measurements, one should bear in mind the following caveats: (1) most local measurements (e.g., in Cappellaro et al. 1999) have been based on photographic data rather than CCD data as used here; (2) we did not apply any correction for host galaxy absorption and inclination; (3) at high redshift, the mix of galaxy types is likely to be very different (which will affect comparisons if different types have differing star formation histories and hence SN Ia rates); and (4) local SN Ia rates are typically reported in SNu, whereas the high-redshift values are more conveniently calculated in "events Mpc^{-3} yr^{-1}" as the rest-frame B-band luminosity is difficult to estimate.

In this section, for the purpose of comparing to the models, we convert local rates from SNu to "events Mpc^{-3} yr^{-1}." To do this, we calculate the B-band luminosity density of the local universe by integrating local B-band luminosity functions (Marzke et al. 1998; Folkes et al. 1999) and find $\rho_{L_B} = (1.7\text{–}2.7) \times 10^8\ h\ L_{B\odot}\ \mathrm{Mpc}^{-3}$; we take an average value in this analysis, but note that this introduces a further uncertainty into the calculation. We convert the local values and plot the results in Figure 7.

To this plot we have added recent theoretical predictions for the form that the evolution of the SN Ia rate might take. Various workers have modeled the expected evolution of the SN Ia rate (Ruiz-Lapuente, Canal, & Burkert 1997;

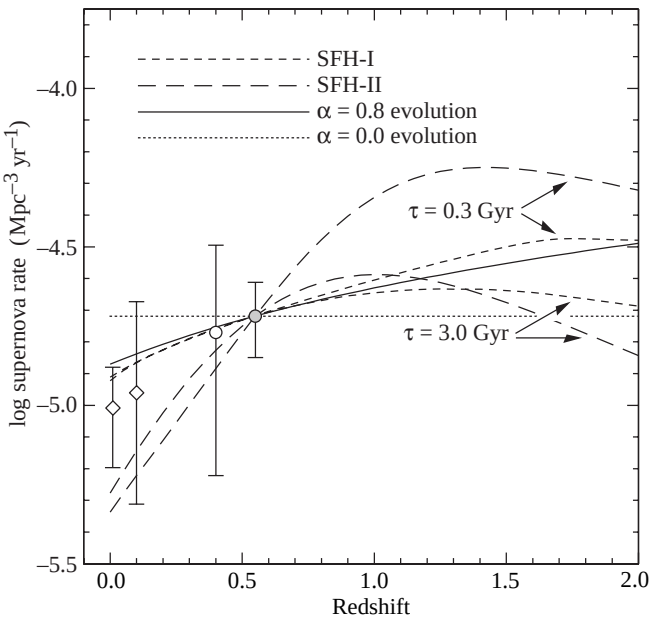

FIG. 7.—SN Ia rate per comoving volume determined here (*filled circle*) compared with that of Paper I (*open circle*) and of Cappellaro et al. (1999) at $z \sim 0.01$ and Hardin et al. (2000) at $z \sim 0.1$ (*open diamonds*). For comparison, theoretical predictions for two SFH scenarios and two delay times are shown; see text for details. Local SN Ia rates have been converted from SNu units. Also shown are an $\alpha = 0.8$ evolution in the SN Ia rate (*solid line*) and the no-evolution case (*dotted line*). The diagram is drawn for $H_0 = 50$ km s^{-1} Mpc and a flat Λ-dominated model with $\Omega_M = 0.3$.

Sadat et al. 1998; Madau et al. 1998; Sullivan et al. 2000a). However, such work is hampered by the uncertain physical nature of the progenitor. The evolution expected depends critically on whether SNe Ia occur in double or single degenerate progenitor systems (for a review see Nomoto et al. 1999 and references therein), the expected evolution in the fraction of stellar binaries, and, of course, the cosmic SFH.

Here we adopt an empirical approach representing these uncertainties in terms of two parameters (Madau et al. 1998; Dahlen & Fransson 1999). The first is a delay time τ between the binary system formation and SN explosion epochs, which defines a time-independent explosion probability per white dwarf. Note that this parameter is treated in different ways in the literature. Madau et al. (1998) define a time-independent explosion probability per white dwarf, which they model as an exponential probability function with a mean value of τ, whereas Dahlen & Fransson (1999) use τ as an *exact* delay time between binary system formation and SN explosion. The difference between the two approaches becomes sizable at higher redshift for scenarios involving large values of τ. Here we adopt the former approach, but note that this may introduce further uncertainties at $z > 1$ in scenarios with large τ. The second parameter is an explosion efficiency, η, which accounts for the fraction of binary systems that never result in an SN. We constrain η by requiring that our predicted rate at $z = 0.55$ is equal to our new observational determination. In Figure 6 we show two illustrative values: $\tau = 0.3$ Gyr, corresponding to a shallower decline at high redshift, and $\tau = 3.0$ Gyr, which produces a steeper drop-off.

We consider each of these two SN Ia models in the context of two different SFH scenarios. The first (SFH-I) is taken from Madau & Pozzetti (2000), who provide a convenient analytical fit of the star formation rate (SFR) form

$$\mathrm{SFR}(z) = \frac{1.67 \times 0.23 e^{3.4z}}{e^{3.8z} + 44.7}\ M_\odot\ \mathrm{yr}^{-1}\ \mathrm{Mpc}^{-3} \qquad (11)$$

in an Einstein–de Sitter universe. We converted this formula to that appropriate for a Λ-dominated flat universe by computing the difference in luminosity density. The SFH fit matches most UV continuum and Hα luminosity densities from $z = 0$ to 4 and includes a mild correction for dust of $A_{1500} = 1.2$ mag ($A_{2800} = 0.55$ mag). However, the SFR evolution in this model to $z \simeq 1.5$ both is stronger and results in a lower local SFR than some recent UV measurements (Cowie, Songaila, & Barger 1999; Sullivan et al. 2000b). Accordingly, we also consider a second SFH (SFH-II) with a shallower evolution (a factor of $\sim$4 from $z = 0$ to 1.75 in an Einstein–de Sitter universe and constant thereafter).

These various predictions are plotted, for a flat $\Omega_M = 0.3$ cosmology, in Figure 7, together with our estimate of the evolutionary index. Although our internal estimate is highly uncertain, already it would seem to favor scenarios that involve little evolution over the redshift range $z = 0$–0.6, a result which is in agreement with comparisons based on the low-redshift rate determinations. Clearly, a precise measurement of the SN Ia rate at, say, $z = 1$ would enable further, more robust constraints to be placed on any evolution, as the redshift range that is currently probed is quite small. In the near future, our Supernova Cosmology Project's ongoing high-redshift SN searches, as well as those of the High-z Supernova Team, should provide enough data at these redshifts to place more stringent constraints on the SFH.

The observations described in this paper were primarily obtained as visiting/guest astronomers at the Cerro Tololo Inter-American Observatory (CTIO) 4 m telescope, operated by the National Optical Astronomy Observatory under contract to the National Science Foundation; the Keck I and II 10 m telescopes of the California Association for Research in Astronomy; the Wisconsin-Indiana-Yale-NOAO (WIYN) telescope; the European Southern Observatory 3.6 m telescope; the Isaac Newton and William Herschel Telescopes, operated on the island of La Palma by the Isaac Newton Group in the Spanish Observatorio del Roque de los Muchachos of the Instituto de Astrofisica de Canarias; the Nordic Optical 2.5 m telescope; and the NASA/ESA *Hubble Space Telescope*, which is operated by the Association of Universities for Research in Astronomy, Inc., under NASA contract NAS 5-26555. We thank the dedicated staff of these observatories for their excellent assistance in pursuit of this project. We thank Gary Bernstein and Tony Tyson for developing and supporting the Big Throughput Camera at the CTIO 4 m; this wide-field camera was important in the discovery of many of the high-redshift SNe. We thank Simon Lilly, Caryl Gronwall, and David Koo for providing their galaxy counts and acknowledge useful discussions with Wal Sargent, Bruno Leibundgut, and Piero Madau. This work was supported in part by the Physics Division, E. O. Lawrence Berkeley National Laboratory of the US Department of Energy under contract DE-AC03-76SF000098, and by the National Science Foundation's Center for Particle Astrophysics, University of California, Berkeley under grant ADT-88909616.

M. S acknowledges support from a Particle Physics and Astronomy Research Council (UK) Fellowship. A. G. is a Royal Swedish Academy Research Fellow supported by a grant from the Knut and Alice Wallenberg Foundation. The France-Berkeley Fund provided additional collaboration support.

REFERENCES

Brinchmann, J. 1999, Ph.D. thesis, Univ. Cambridge
Brinchmann, J., et al. 1998, ApJ, 499, 112
Burstein, D., & Heiles, C. 1982, AJ, 87, 1165
Cappellaro, E., Evans, R., & Turatto, M. 1999, A&A, 351, 459
Cardelli, J. A., Clayton, G. C., & Mathis, J. S. 1989, ApJ, 345, 245
Carroll, S. M., Press, W. H., & Turner, E. L. 1992, ARA&A, 30, 499
Cowie, L., Songaila, A., & Barger, A. J. 1999, AJ, 118, 603
Dahlen, T., & Fransson, C. 1999, A&A, 350, 349
Folkes, S., et al. 1999, MNRAS, 308, 459
Garnavich, P. M., et al. 1998, ApJ, 493, L53
Gibson, B. K., et al. 2000, ApJ, 529, 723
Gronwall, C., & Koo, D. 1995, ApJ, 440, L1
Gunn, S., Hoessel, L., & Oke, B. 1986, ApJ, 306, 30
Hamuy, M., Phillips, M. M., Schommer, R. A., Suntzeff, N. B., Maza, J., & Aviles, R. 1996, AJ, 112, 2391
Hardin, D., et al. 2000, A&A, 362, 419
Kim, A., Goobar, A., & Perlmutter, S. 1996, PASP, 108, 190
Landolt, A. U. 1992, AJ, 104, 340
Leibundgut, B. 1988, Ph.D. thesis, Univ. Basel
———. 2001, ARA&A, 39, 67
Lilly, S., Tresse, L., Hammer, F., Crampton, D., & Le Fevre, O. 1995, ApJ, 455, 108
Loveday, J., Peterson, B. A., Efstathiou, G., & Maddox, S. J. 1992, ApJ, 400, L43
Madau, P., Della Valle, M., & Panagia, N. 1998, MNRAS, 297, L17
Madau, P., & Pozzetti, L. 2000, MNRAS, 312, L9
Marzke, R. O., da Costa, L. N., Pellegrini, P. S., Willmer, C. N. A., & Geller, M. J. 1998, ApJ, 503, 617
McMahon, R. G., & Irwin, M. J. 1992, in Digitized Optical Sky Surveys, ed. H. T. MacGillivray & E. B. Thomson (Dordrecht: Kluwer), 417
Nomoto, K., Umeda, H., Hachisu, I., Kato, M., Kobayashi, C., & Tsujimoto, T. 1999, in Type Ia Supernovae: Theory and Cosmology, ed. J. C. Niemeyer & J. W. Truran (Cambridge: Cambridge Univ. Press), Chap. 6
Oke, J. B., et al. 1995, PASP, 107, 375
Pain, R., et al. 1996, ApJ, 473, 356 (SCP Collaboration) (Paper I)
Peacock, J. A., et al. 2001, Nature, 410, 169
Perlmutter, S., et al. 1995a, IAU Circ. 6270 (SCP Collaboration)
———. 1995b, in Thermonuclear Supernova, ed. P. Ruiz-Lapuente, R. Canal, & J. Isern (Dordrecht: Kluwer), 749 (SCP Collaboration)
———. 1996, IAU Circ. 6621 (SCP Collaboration)
———. 1997a, ApJ, 483, 565 (SCP Collaboration)
———. 1997b, IAU Circ. 6596 (SCP Collaboration)
———. 1997c, IAU Circ. 6804 (SCP Collaboration)
———. 1998, Nature, 391, 51 (erratum 392, 311) (SCP Collaboration)
———. 1999, ApJ, 517, 565 (SCP Collaboration)
Phillips, M. M. 1993, ApJ, 413, L105
Phillips, M. M., Lira, P., Suntzeff, N. B., Schommer, R. A., Hamuy, M., & Maza, J. 1999, AJ, 118, 1766
Poggianti, B. 1997, A&AS, 122, 399
Reiss, D. J. 2002, Ph.D. thesis, Univ. Washington
Riess, A. G., et al. 1998, AJ, 116, 1009
Riess, A. G., Press, W. H., & Kirshner, R. P. 1996, ApJ, 473, 88
Ruiz-Lapuente, P., & Canal, R. 1998, ApJ, 497, L57
Ruiz-Lapuente, P., Canal, R., & Burkert, A. 1997, in Thermonuclear Supernovae, ed. P. Ruiz-Lapuente, R. Canal, & J. Isern (Dordrecht: Kluwer), 205
Sadat, R., Blanchard, A., Guiderdoni, B., & Silk, J. 1998, A&A, 331, L69
Saha, A., Sandage, A., Tammann, G. A., Labhardt, L., Macchetto, F. D., & Panagia, N. 1999, ApJ, 522, 802
Schlegel, D., Finkbeiner, D., & Davis, M. 1998, ApJ, 500, 525
Schmidt, B. P., et al. 1998, ApJ, 507, 46
Sullivan, M., Ellis, R., Nugent, P., Smail, I., & Madau, P. 2000a, MNRAS, 319, 4549
Sullivan, M., Treyer, M., Ellis, R. S., Bridges, T., Donas, J., & Milliard, B. 2000b, MNRAS, 312, 442
Wittman, D. M., Tyson, J. A., Bernstein, G. M., Lee, R. W., dell'Antonio, I. P., Fischer, P., Smith, D. R., & Blouke, M. M. 1998, Proc. SPIE, 3355, 626
Yungelson, L., & Livio, M. 1998, ApJ, 497, 168